

A porous cobalt(II)-organic framework exhibiting high room temperature proton conductivity and field-induced slow magnetic relaxation

Yue Zhou,^{a†} Shruti Moorthy,^{c†} Xiao-Qin Wei,^{*b} Saurabh Kumar Singh,^{*c} Zhengfang Tian^a and Dong Shao^{a,d*}

^a *Hubei Key Laboratory of Processing and Application of Catalytic Materials, College of Chemistry and Chemical Engineering, Huanggang Normal University, Huanggang 438000, P. R. China.*

^c *Department of Material Science and Engineering, Shanxi Province Collaborative Innovation Center for Light Materials Modification and Application, Jinzhong University, Jinzhong, 030619, P. R. China.*

^b *Department of Chemistry, Indian Institute of Technology Hyderabad, Kandi-502285, Sangareddy, Telangana, India.*

^d *State Key Laboratory of Coordination Chemistry, Nanjing University, Nanjing, 210023, P. R. China.*

† Y. Z. and S. M. contributed equally to this work.

Correspondence and requests for materials should be addressed to

Email: shaodong@nju.edu.cn or sksingh@chy.iith.ac.in

Table of Contents

EXPERIMENTAL SECTION	4
Table S1. Structural and magnetic parameters of reported 2D SIMs.	7
Table S2. Crystallographic data and structure refinement parameters for 1 at different measured temperature.	8
Table S3. Selected bond lengths (\AA) and angles [$^\circ$] in 1	9
Figure S1. The asymmetric units of 1 measured at different temperatures.	10
Table S4. Continuous Shape Measure (CSM) analysis for six-coordinated Co(II) in 1	10
Table S5. The possible hydrogen bonds in 1 at 123 K calculated by PLATON.	11
Table S6. The possible hydrogen bonds in 1 at 193 K calculated by PLATON.	11
Table S7. The possible hydrogen bonds in 1 at 293 K calculated by PLATON.	12
Table S8. The possible hydrogen bonds in 1 at 323 K calculated by PLATON.	12
Figure S2. Intermolecular $\pi \cdots \pi$ distances between benzimidazole molecules 1	13
Figure S3. The anisotropic thermomechanical behavior of 1	13
Figure S4. Comparison of the experimental PXRD pattern at room temperature of 1 with the simulated pattern from single crystal structure at 293 K.....	14
Figure S5. Frequency dependence of the ac susceptibilities measured under zero dc field at 2.0 K for 1	14
Figure S6. Frequency dependence of the in-phase (χ') and out-of-phase (χ'') magnetic susceptibility of 1 measured at 1.8 K in various applied fields from 0 to 3000 Oe.	15
Figure S7. Cole–Cole plots of χ' vs. χ'' of 1 at 2.0 K under various applied dc fields. The solid lines represent the best fit of the experimental results with the generalized Debye model....	15
Table S9. Relaxation fitting parameters at 2.0 K under different fields from the least-square fitting of the Cole-Cole plots of 1 according to the generalized Debye model.	16
Figure S8. Field dependence of the magnetic relaxation time at 2.0 K for 1	16
Figure S9. Frequency dependence of the in-phase (χ') and out-of-phase (χ'') ac susceptibilities measured under 1 kOe dc field in the temperature range of 2.0 – 10 K for 1	17
Figure S10. Cole-Cole plots of 1 obtained from 1 kOe dc field. The solid lines represent the best fits according to the generalized Debye model.	17
Table S10. Relaxation fitting parameters from the least-square fitting of the Cole-Cole plots of 1 under 1 kOe dc filed according to the generalized Debye model.	18
COMPUTATIONAL DETAILS.....	19
Table S11. CASSCF/NEVPT2 computed 10 spin-free quartet (red) and 40 spin-free doublet (blue) states along the spin-orbit states for Co centre in complex 1a . All the values are reported here in cm^{-1}	20
Table S12. CASSCF (7,5)+NEVPT2 computed Spin – Hamiltonian parameter (g, D, E/D) along with listed state – by – state contribution to the D. All the values are reported here in cm^{-1}	21

Table S13. AILFT derived ligand field parameters computed at NEVPT2 level of theory for model complexes 1. The values of B, C, ξ and Δ_o parameters are provided in units of cm ⁻¹ .	21
Table S14. NEVPT2-AILFT computed d-orbital ordering for model complexes 1.....	21
Figure S12. Experimental and ab initio computed molar magnetic susceptibility plots where red circles correspond to the experimental values and the blue and black lines correspond to CASSCF and NEVPT2 computed values.....	22
Figure S11. NEVPT2 computed orientation of computed effective g-tensor and D-tensor for complex 1 . Color code: Co(cyan), N (blue), C (grey), O(red), H(white).	22
Figure S13. Solid-state UV-vis-NIR of 1	23
References	24

EXPERIMENTAL SECTION

Materials. All reagents were commercially available and used as received without further purification. The powder of the starting material 1H-benzimidazole-5-carboxylic acid (**H₂bic**) was directly purchase from Tokyo Chemical Industry (TCI).

Synthesis of {[Co(Hbic)(H₂O)]·4H₂O}_n (1)}

A mixture of **H₂bic** (0.2 mmol, 32.4 mg) and Co(ClO₄)₂·6H₂O (0.1 mmol, 36.6 mg) was dissolved in 6 ml H₂O. The reaction mixture was stirred at room temperature for several minutes, which was placed in a 15 mL Pyrex glass tube and heated in an oven at 100 °C for three days. Then, the reaction system was cooled to ambient temperature via a programmed cooling process (15 °C per hour). A day later, single-phase orange single crystals were obtained. The product was isolated by filtration, washed with the mother liquor, and air-dried. Yield: 21 mg, ca. 44.6%. Elemental analysis (%) for C₁₆H₂₀CoN₄O₉: C, 40.78; H, 4.28; N, 11.89. Found: C, 40.82, H, 4.41; N, 11.79. IR (KBr, cm⁻¹): 3510-3110 (bs), 2921 (s), 1655 (s), 1614(s), 1600(s), 1554(s), 1464(w), 1424(w), 1392(vs), 1284(s), 967 (w), 786 (m), 761(w), 596 (w) cm⁻¹. Solid-state UV-vis-NIR: 638 nm, 1040 nm (Fig. S13).

Physical measurements

Elemental analyses of C, H, and N were performed at an Elementar Vario MICRO analyzer. Infrared spectra were obtained in the range of 600–4000 cm⁻¹ on a Bruker tensor II spectrometer. Solid-state vis-NIR spectra were obtained on the samples at room temperature using a CARY5000 spectrophotometer equipped with a Harrick Praying Mantis accessory. Variable-temperature powder X-ray diffraction data (PXRD) were recorded on a Bruker D8 Advance diffractometer with Cu K α X-ray source ($\lambda = 1.54056 \text{ \AA}$) operated at 40 kV and 40 mA between 5 and 35° (2θ). Simulated PXRD patterns were obtained from the Mercury software. Thermal gravimetric analysis (TGA) was carried out on freshly filtered crystals using the Mettler Toledo TGA2 instrument in an insert Ar atmosphere over a temperature range of 27–700 °C with a heating rate of 10 °C/min. Low-pressure volumetric N₂ gas adsorption measurements were

performed on a Quadrasorb automatic volumetric instrument. The samples were activated in dynamic vacuum at 150 °C for 24 h before measurement. The Brunauer-Emmett-Teller (BET) method was utilized to calculate the specific surface areas. Water adsorption/desorption isotherms were measured using a BELSORP max instrument. Proton conductivity measurements were performed using a quasi-four-electrode AC impedance technique with a Solartron 1260 impedance/gain-phase analyzer. The single crystals samples were compressed to 2.5 mm diameter, which were connected to gold wires using silver paste. The sample pellet was measured in the temperature range of 25–50 °C and in the RH range of 40–95%. The conductivity of the samples was deduced from the Debye semicircle in the Nyquist plot.

Magnetic measurements

Direct current (dc) magnetic susceptibility from 2 to 300 K with applied 1000 Oe dc field were performed using a Quantum Design SQUID VSM magnetometer on the crushed single crystals sample of **1**. Alternative current (ac) magnetic susceptibility data were collected in a zero-dc field or an applied 1000 Oe dc fields in the temperature range of 2-10 K, under an ac field of 2 Oe, oscillating at frequencies in the range of 1-1000 Hz. All magnetic data were corrected for the diamagnetic contributions of the sample holder and of core diamagnetism of the sample using Pascal's constants.

X-ray Crystallography

Single crystal X-ray diffraction data were collected on a Bruker D8 QUEST diffractometer with a PHOTON III area detector (Mo-K α radiation, $\lambda = 0.71073 \text{ \AA}$, Bruker *Ius* 3.0) at room temperature. The APEX III program was used to determine the unit cell parameters and for data collection. The data were integrated and corrected for Lorentz and polarization effects using SAINT.^{S1} Absorption corrections were applied with SADABS.^{S2} The structures were solved by direct methods and refined by full-matrix least-squares method on F^2 using the SHELXTL^{S3} crystallographic software package integrated in Olex 2.^{S4} All the non-hydrogen atoms were refined anisotropically. Hydrogen atoms of the organic ligands were refined as riding on the corresponding non-hydrogen atoms. Additional details of the data collections and structural refinement parameters are provided in Table 1. Selected bond lengths and

angles of **1** were listed in Table S2, S3. CCDC 2208435-2208438 are the supplementary crystallographic data for this paper. They can be obtained freely from the Cambridge Crystallographic Data Centre via www.ccdc.cam.ac.uk/data_request/cif.

Table S1. Structural and magnetic parameters of reported 2D SIMs.

Complexes	Geometry	Closest Co-Co distance (Å)	D (cm ⁻¹)	U _{eff} (K)	Ref.
[Co(ppad) ₂] _n	O _h	8.302	+76	16.4	S1
[Co(dca) ₂ (atz) ₂] _n	O _h	8.602	/	7.3	S2
{[Co(bmzbc) ₂]·2DMF} _n	O _h	8.32	+62.6	11.8	S3
[Co(L) ₂ (SCN) ₂ ·2(CH ₃ CN)·2(dmf)] _n	O _h	13.028	+41.6	36.9	S4
{[Co(3,3'-Hbpt) ₂ (SCN) ₂]·2H ₂ O} _n	O _h	9.854	+70.1	33.5	S5
[Co(dca) ₂ (bim) ₂] _n	O _h	8.927(2)	+74.3	7.7	S6
[Co(dca) ₂ (bmim) ₂] _n	O _h	8.7110(5)	+75.8	19.9	S6
[Co(bpeb) ₂ (NCS) ₂]·nG (G= DCB)	O _h		+64.9(9)	45.1	S7
[Co(bpeb) ₂ (NCS) ₂]·nG (G= TAN)	O _h		+67.1(9)	24.6	S7
[Co(bpeb) ₂ (NCS) ₂]·nG (G= TOL)	O _h		+84.4(4)	16.56	S7
[Co(bpeb) ₂ (NCS) ₂]·nG (G= PYR)	O _h		+70.3(9)	30.24	S7
[Co(bmzbc) ₂ (1,2-etdio)] _n	O _h	8.61	/	16.7	S8
[Co(bmzbc) ₂ (Hbmzbc)] _n	O _h	7.73	/	31.2	S8
{[Co(HL)(bpy)(H ₂ O) ₂]·DMF} _n	O _h	11.36	-0.071	13.9	S9
{[Co(HL)(bpe)]·0.5bpe} _n	O _h	10.86	-0.076	8.7	S9
[Co(μ-6ani) ₂]·H ₂ O	O _h	7.099	+28	18.7	S10
{[Co ^{II} (TPT) _{2/3} (H ₂ O) ₄][CH ₃ COO] ₂ ·(H ₂ O) ₄ } _n	O _h	8.293	+47.7	6.912	S11
[Co ^{III} (CN) ₆] ₂ [Co ^{II} (TODA)] ₃ ·9H ₂ O	D _{5h}	7.58	+29.9	16	S12
[Co(bpg) ₂ (SCN) ₂]·3MeOH	O _h	9.110	+64.2	5.0	S13
[Co(bpg) ₂ (SCN) ₂]·2DMF	O _h	8.544	+67.5	15.3	S13
[Co(1,4-bimb) _{0.5} (5-aip)(H ₂ O)] _n	O _h	5.7874	/	4.9	S14
[Co(dps) ₂ Cl ₂] _n	O _h	7.500	27.2	12.4	S15
[Co(dps) ₂ Br ₂] _n	O _h	8.992	28.0	27.1	S15
[Co(dps) ₂ (H ₂ O) ₂ ·I ₂ ·(H ₂ O) ₄ } _n	O _h	7.534	9.5	28.8	S15
{Co(DMSO) ₂ [Au(CN) ₂] ₂ } _n	O _h	10.344	+68	22.1	S16
{Co(DMF) ₂ [Au(CN) ₂] ₂ } _n	O _h	7.557	+90	18.5	S16
{Co(PY) ₂ [Au(CN) ₂] ₂ } _n	O _h	7.135	+75	22.0	S16
{Co(PyPhCO) ₂ [Au(CN) ₂] ₂ } _n	O _h	7.436	+80	15.9	S16
[Co(m-NPy3)(TPA)0.5Cl·CH ₃ OH] _n	O _h	9.89	/	9.89	S17
{[Co(IPEH) ₂ (SCN) ₂]·H ₂ O} _n	O _h	8.397	89.3	6.5	S18
[Co(Hbic) ₂] _α	T _d	7.912	-20.4	24.9	S19
[Co(Hbic) ₂] _β	T _d	7.487	-14.6	4.3	S19
{Co ₂ (DCIQ) ₄ (tpb)} _n	O _h	9.064	-46.0	23.5	S20

Ppad, N3-(3-pyridoyl)-3-pyridinecarboxamidrazone; **dca**, dicyanamide; **atz**, 2-amino1,3,5-triazine; **bmzbc⁻**, 4-(benzimidazole-1-yl)benzoate; L = 4'-(4-methoxyphenyl)-4,2':6',4''-terpyridine; **3,3'-Hbpt**, 1H-3-(3-pyridyl)-5-(30-pyridyl)-1,2,4-triazole; **dca**, dicyanamide; **bim** = 1-benzylimidazole; **bmim** = 1-benzyl-2-methylimidazole; **6ani**, 6-aminonicotinate; **TPT**, 2,4,6-Tris(4-pyridyl)-1,3,5-triazine; **bpg** = meso- α,β -bi(4-pyridyl) glycol; **1,2-etdio**, 1,2-ethanediol; **Hbmzbc**, 4-(benzimidazole-1-yl)benzoic acid; **6ani**, 6-aminonicotinate; TPT, 2,4,6-Tris(4-pyridyl)-1,3,5-triazine; **bpg**, meso- α,β -bi(4-pyridyl) glycol; **dps**, 4,4'-dipyridyl sulfide; PyPhCO, benzoylpyridine; **TPA** = bidentate terephthalic acid; **m-NPy3**, tris(4-(pyridine-3-yl)phenyl)amine ligand; **IPEH**, (((1E,2E)-1,2-bis(1-(4-(1H-imidazol-1-yl)phenyl)ethylidene)hydrazine; **tpb** = 1,2,4,5-tetra(4-pyridyl)benzene; **DCIQ** = (5,7-dichloro-8-hydroxyquinoline).

Table S2. Crystallographic data and structure refinement parameters for **1** at different measured temperature.

Complex	1			
Empirical formula	$\text{C}_{16}\text{H}_{20}\text{CoN}_4\text{O}_9$			
Formula weight	471.29			
<i>T</i> / K	123	193	293	323
Crystal system	triclinic			
Space group	<i>P</i> \bar{I}			
a/Å	8.8988(6)	8.8963(7)	8.8974(6)	8.8812(14)
b/Å	9.8033(6)	9.8095(8)	9.8135(6)	9.8009(15)
c/Å	11.4213(7)	11.4439(9)	11.4695(7)	11.4837(17)
α /°	90.342(2)	90.451(3)	90.505(2)	91.074(4)
β /°	103.096(2)	102.942(3)	102.776(2)	102.543(4)
γ /°	104.310(2)	103.990(3)	103.451(2)	103.688(5)
Volume/Å ³	938.31(10)	942.42(13)	947.95(10)	945.4(3)
Z	2	2	2	2
ρ_{calcg} /cm ³	1.668	1.661	1.651	1.656
μ /mm ⁻¹	0.976	0.971	0.966	0.968
F(000)	486	486	486	486
2Θ range for data collection/°	4.298 to 51.422	4.288 to 51.49	4.276 to 52.858	4.29 to 53.118
Reflections collected	36302	30488	37643	42636
Independent reflections	3572	3587	3889	3944
$R_{\text{int}} / R_{\text{sigma}}$	0.1123 / 0.0516	0.0518/0.0251	0.0987/0.0480	0.1446/0.0690
Goodness-of-fit on F^2	1.056	1.036	1.030	1.022
$R_1^{\text{a}} / wR_2^{\text{b}}$ ($I > 2\sigma(I)$)	0.0654 / 0.1655	0.0589/ 0.1537	0.0620/0.1666	0.643/0.1598
R_1 / wR_2 (all data)	0.0899 /0.1823	0.0666/ 0.1606	0.0821/0.1848	0.1094/0.1850
Max/min [e Å ⁻³]	1.01 / -0.95	1.16 / -0.88	0.89/-0.89	0.64/-0.59

^a $R_1 = \sum ||F_0| - |F_c|| / \sum |F_0|$ ^b $wR_2 = \{\sum [w(F_o^2 - F_c^2)^2] / \sum [w(F_o^2)^2]\}^{1/2}$

Table S3. Selected bond lengths (Å) and angles [°] in **1**.

Parameter	Value / Å, °			
T / K	123	193	293	323
Co1-O1	2.054(3)	2.050(3)	2.047(3)	2.045(3)
Co1-O3	2.138(3)	2.140(3)	2.140(3)	2.153(3)
Co1-O4 ¹	2.230(3)	2.230(3)	2.236(3)	2.238(3)
Co1-O5 ¹	2.173(4)	2.174(3)	2.179(3)	2.178(4)
Co1-N ¹	2.113(4)	2.115(3)	2.114(4)	2.114(4)
Co1-N4 ²	2.102(4)	2.100(3)	2.103(4)	2.095(4)
O1-Co1-O3	90.40(13)	90.40(11)	90.61(12)	90.69(13)
O1-Co1-O4 ¹	151.36(14)	151.09(12)	150.85(13)	150.79(14)
O1-Co1-O5 ¹	91.93(14)	91.82(11)	91.76(12)	91.54(14)
O1-Co1-N1	103.08(15)	103.19(12)	103.13(13)	103.80(15)
O3-Co1-N4 ¹	84.21(13)	84.23(11)	84.03(12)	84.22(13)
O5 ¹ -Co1-O4 ¹	59.73(13)	59.58(11)	59.41(11)	59.52(13)
N1-Co1-O3	92.65(14)	92.18(12)	92.04(13)	92.25(14)
N4 ² -Co1-O3	174.62(15)	174.87(13)	174.98(13)	175.07(15)
N4 ² -Co1-N1	91.48(16)	91.63(13)	91.48(14)	91.41(16)

Symmetry operation: ¹ +X, -1 + Y, + Z; ² 1 + X, + Y, + Z

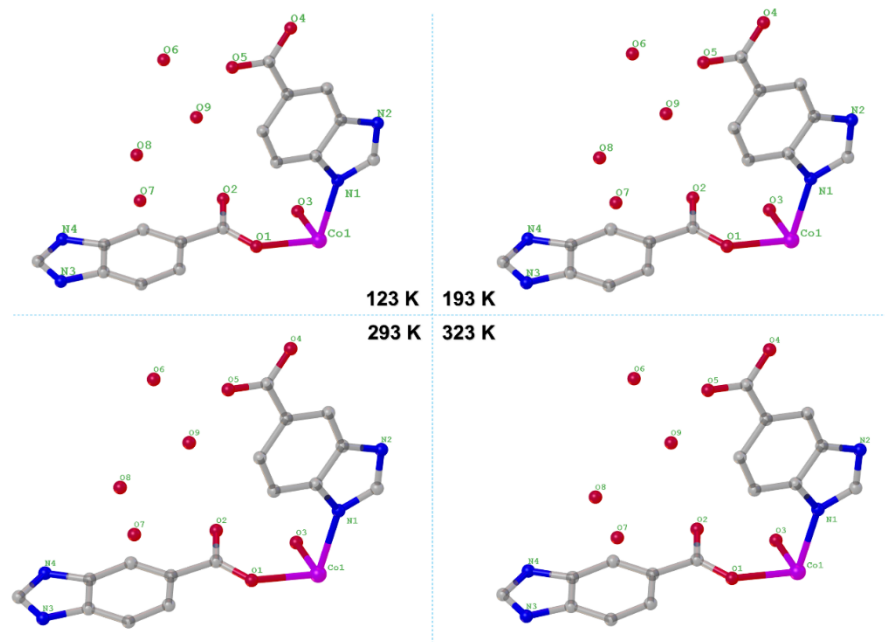


Figure S1. The asymmetric units of **1** measured at different temperatures.

Table S4. Continuous Shape Measure (CSM) analysis for six-coordinated Co(II) in **1**.

Compound, Metal center	T / K	CSM parameters*					Determined coordination geometry	
		six-coordinated coordination sphere						
		HP-6	PPY-6	OC-6	TPR-6	JPPY-6		
Co1	123	30.837	23.083	2.104	13.672	26.934	OC-6	
	193	30.764	22.959	2.138	13.624	26.787		
	293	30.649	22.790	2.171	13.584	26.596		
	323	30.794	22.951	2.161	13.478	26.753		

*CSM^{S2} parameters for six-coordinated complexes:

HP-6 - the parameter related to the hexagon (D_{6h})

PPY-6 - the parameter related to the pentagonal pyramid (C_{5v})

OC-6 - the parameter related to the octahedron (O_h)

TPR-6 - the parameter related to the trigonal prism (D_{3h})

JPPY-6 - the parameter related to the Johnson pentagonal pyramid ($C5v$)

Table S5. The possible hydrogen bonds in **1** at 123 K calculated by PLATON.

D-H...A	d(D- H)	d(H...A)	d(D...A)	<(DHA)
N(2)-H(2)...O(9)	0.86	2.01	2.8358	160
N(3)-H(3)...O6)	0.86	2.04	2.8791	165
O(3)-H(3A)...O(2)	0.87	1.85	2.6072	147
O(3)-H(3B)...O(4)	0.85	1.87	2.7053	164
O(6)-H(6A)...O(9)	0.84	2.10	2.8596	149
O(6)-H(6B)...O(3)	0.85	2.46	3.2114	148
O(7)-H(7A)...O(8)	0.85	1.86	2.6617	157
O(7)-H(7A)...O(7)	0.85	2.22	2.5903	107
O(7)-H(7B)...N(3)	0.85	2.49	3.2815	156
O(9)-H(9B)...O(2)	0.84	1.98	2.7547	153

Table S6. The possible hydrogen bonds in **1** at 193 K calculated by PLATON.

D-H...A	d(D- H)	d(H...A)	d(D...A)	<(DHA)
N(2)-H(2)...O(9)	0.86	2.02	2.8423	159
N(3)-H(3)...O6)	0.86	2.05	2.8905	164
O(3)-H(3A)...O(2)	0.87	1.85	2.6091	145
O(3)-H(3B)...O(4)	0.85	1.87	2.7081	163
O(6)-H(6A)...O(9)	0.84	2.11	2.8811	150
O(6)-H(6B)...O(3)	0.85	2.47	3.2155	148
O(7)-H(7A)...O(8)	0.85	1.74	2.5016	148
O(7)-H(7B)...N(3)	0.85	2.55	3.3672	162
O(9)-H(9B)...O(2)	0.84	1.98	2.7607	154

Table S7. The possible hydrogen bonds in **1** at 293 K calculated by PLATON.

D-H...A	d(D- H)	d(H...A)	d(D...A)	<(DHA)
N(2)-H(2)...O(9)	0.86	2.03	2.8358	160
N(3)-H(3)...O6)	0.86	2.06	2.8791	165
O(3)-H(3A)...O(2)	0.87	1.87	2.6072	143
O(3)-H(3B)...O(4)	0.87	1.87	2.7053	163
O(6)-H(6A)...O(9)	0.85	2.16	2.8596	152
O(6)-H(6B)...O(3)	0.85	2.49	3.2114	147
O(7)-H(7A)...O(8)	0.85	1.54	2.6617	138
O(7)-H(7B)...N(3)	0.85	2.54	3.2815	159
O(9)-H(9A)...N(2)	0.84	2.51	2.8505	105
O(9)-H(9B)...O(2)	0.85	2.00	2.7682	150

Table S8. The possible hydrogen bonds in **1** at 323 K calculated by PLATON.

D-H...A	d(D- H)	d(H...A)	d(D...A)	<(DHA)
N(2)-H(2)...O(9)	0.86	2.05	2.8683	160
N(3)-H(3)...O(5)	0.86	2.53	3.0468	120
N(3)-H(3)...O(6)	0.86	2.11	2.9411	162
O(3)-H(3A)...O(2)	0.87	1.86	2.6080	143
O(3)-H(3B)...O(4)	0.87	1.87	2.7146	165
O(6)-H(6A)...O(9)	0.85	2.52	2.9046	108
O(6)-H(6B)...O(3)	0.85	2.49	3.1975	141
O(8)-H(8A)...N(3)	0.85	2.46	3.2134	148
O(9)-H(9A)...N(2)	0.85	2.28	2.8683	126
O(9)-H(9B)...O(2)	0.85	2.01	2.7737	149

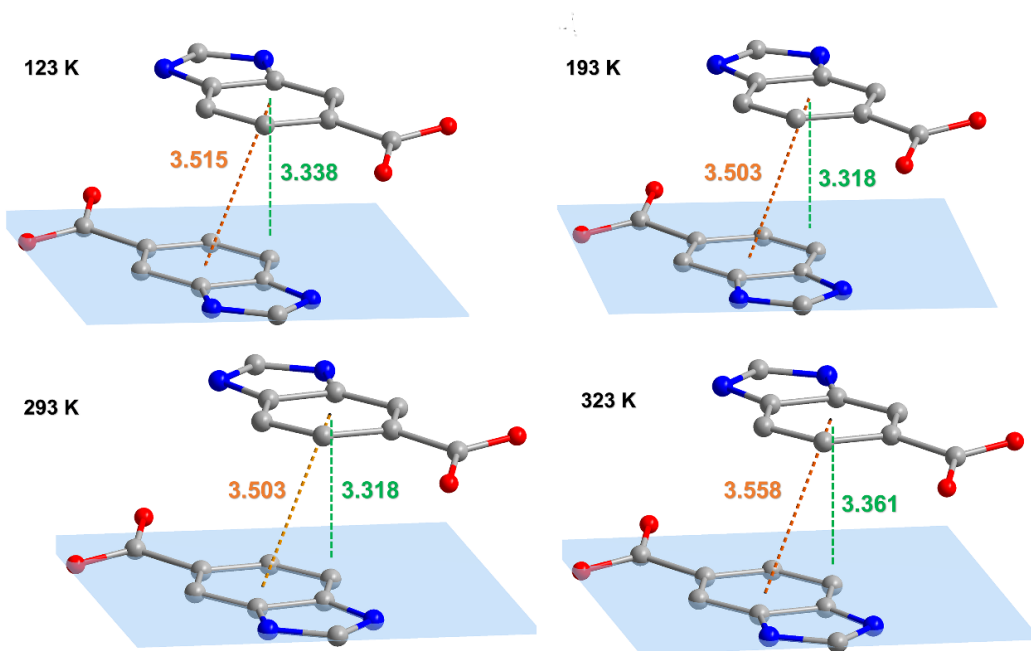


Figure S2. Intermolecular $\pi\cdots\pi$ distances between benzimidazole molecules **1**.

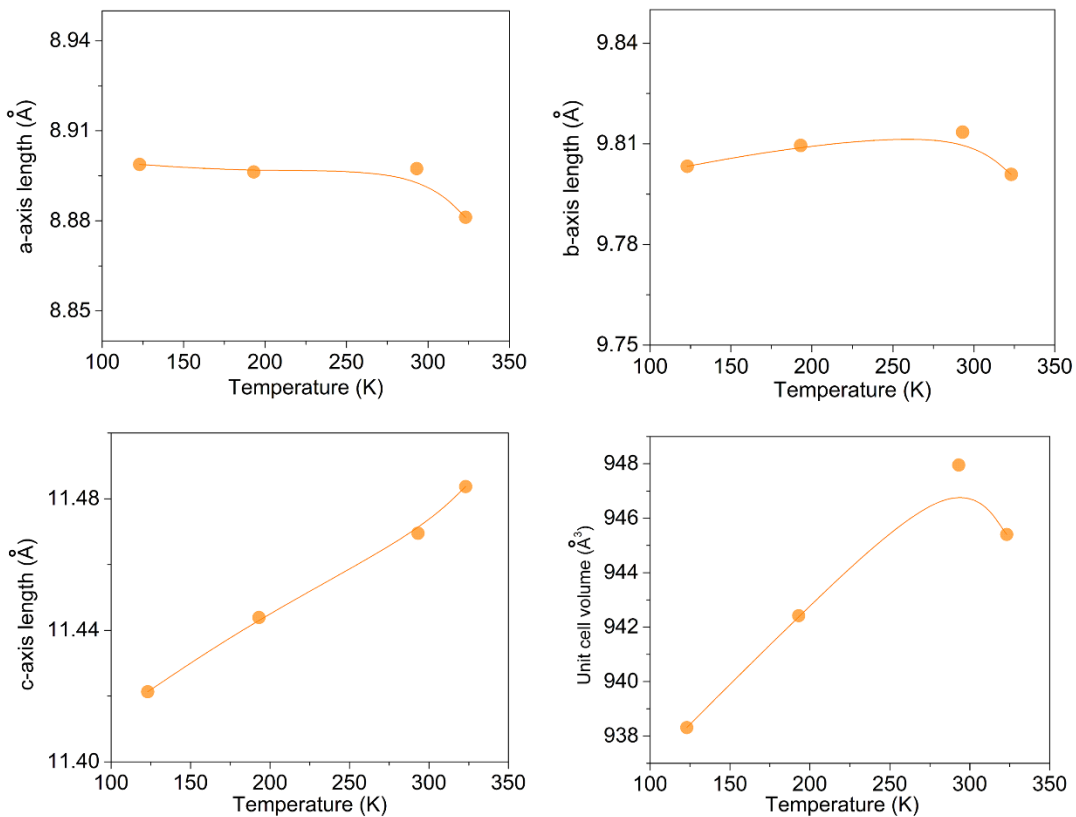


Figure S3. The anisotropic thermomechanical behavior of **1**.

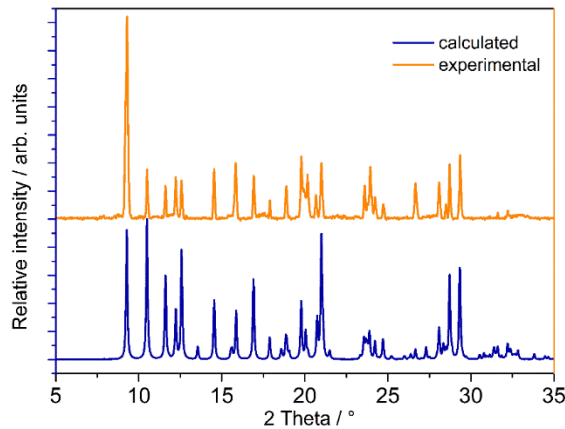


Figure S4. Comparison of the experimental PXRD pattern at room temperature of **1** with the simulated pattern from single crystal structure at 293 K.

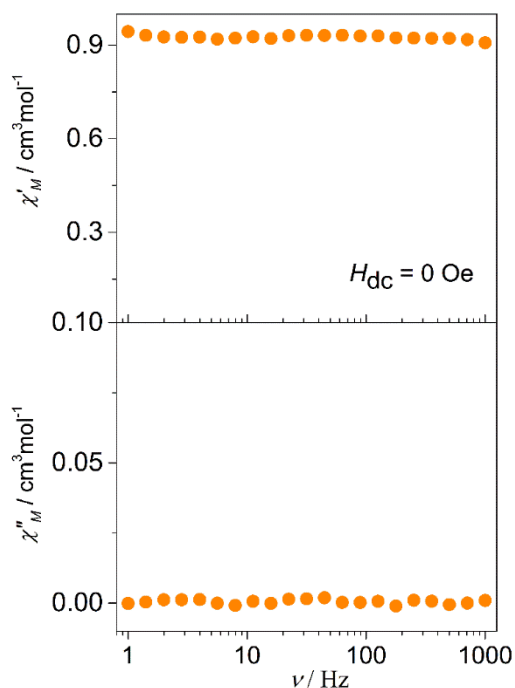


Figure S5. Frequency dependence of the ac susceptibilities measured under zero dc field at 2.0 K for **1**.

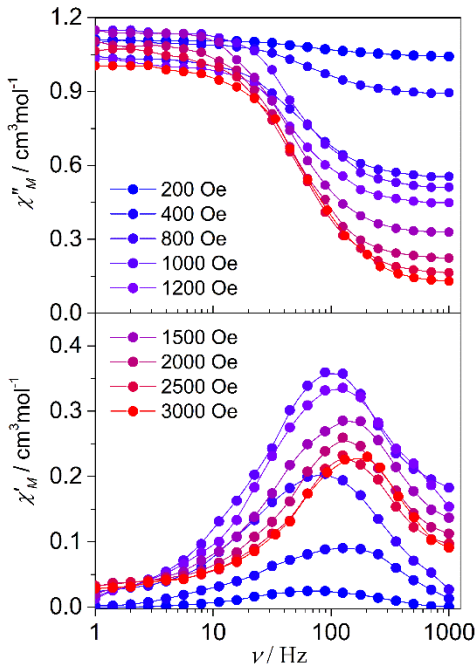


Figure S6. Frequency dependence of the in-phase (χ') and out-of-phase (χ'') magnetic susceptibility of **1** measured at 1.8 K in various applied fields from 0 to 3000 Oe.

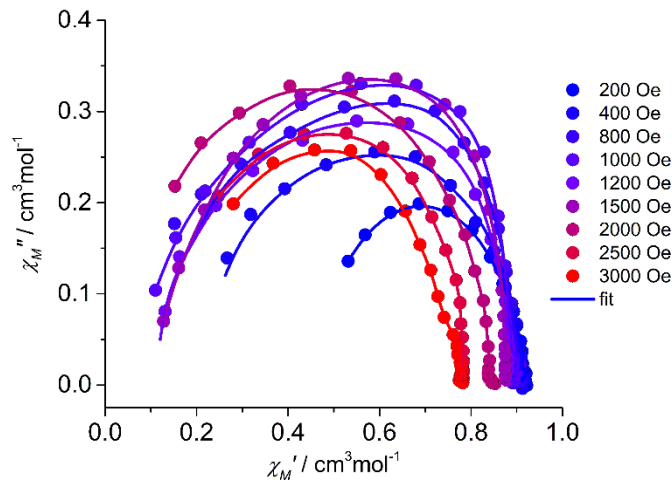


Figure S7. Cole–Cole plots of χ' vs. χ'' of **1** at 2.0 K under various applied dc fields. The solid lines represent the best fit of the experimental results with the generalized Debye model.

Table S9. Relaxation fitting parameters at 2.0 K under different fields from the least-square fitting of the Cole-Cole plots of **1** according to the generalized Debye model.

H / Oe	χ_s / $\text{cm}^3\text{mol}^{-1}\text{K}$	χ_T / $\text{cm}^3\text{mol}^{-1}\text{K}$	τ / s	α
200	0.54433	0.91216	4.5E-4	0.11021
400	0.23783	0.92901	5.7E-4	0.0819
800	0.20008	0.90461	7.1E-4	0.08204
1000	0.07203	0.91261	6.4E-4	0.11467
1200	0.09686	0.88107	6.6E-4	0.02572
1500	0.11278	0.93018	9.1E-4	0.10531
2000	0.10157	0.82412	4.2E-4	0.05941
2500	0.15103	0.78419	3.7E-4	0.02231
3000	0.18047	0.76184	3.5E-4	0.03081

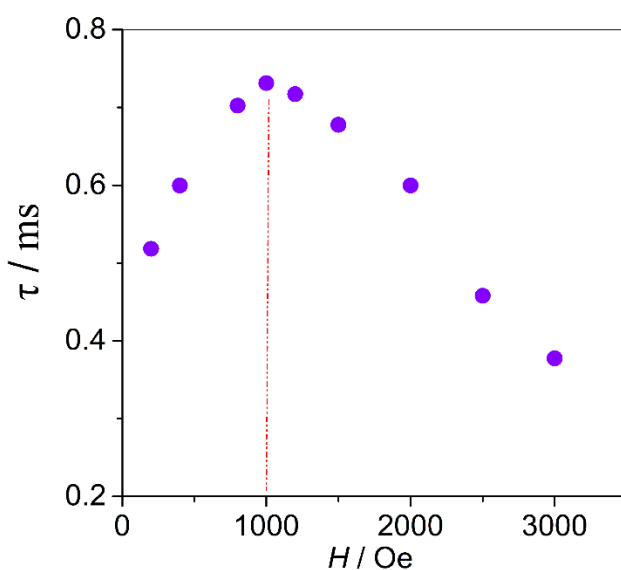


Figure S8. Field dependence of the magnetic relaxation time at 2.0 K for **1**.

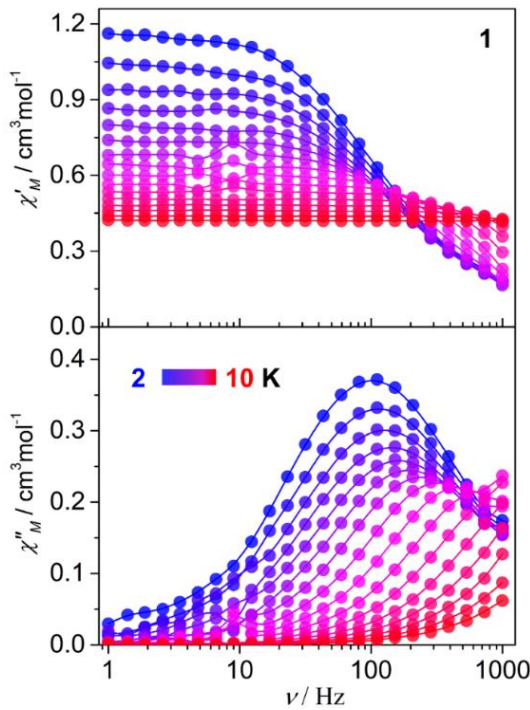


Figure S9. Frequency dependence of the in-phase (χ') and out-of-phase (χ'') ac susceptibilities measured under 1 kOe dc field in the temperature range of 2.0 – 10 K for **1**.

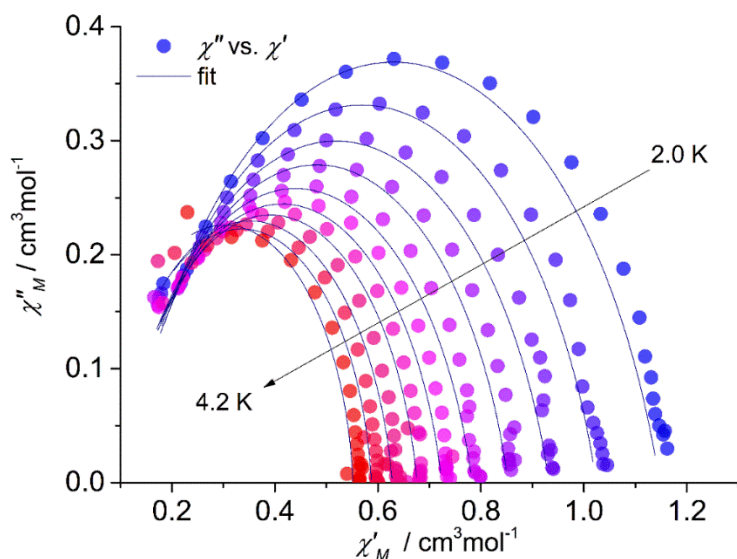


Figure S10. Cole-Cole plots of **1** obtained from 1 kOe dc field. The solid lines represent the best fits according to the generalized Debye model.

Table S10. Relaxation fitting parameters from the least-square fitting of the Cole-Cole plots of 1 under 1 kOe dc filed according to the generalized Debye model.

T / K	τ / s	χ_s / cm ³ mol ⁻¹ K	χ_T / cm ³ mol ⁻¹ K	α
1.99996	0.00147	0.11446	1.14691	0.20983
2.25002	0.0013	0.11349	1.02411	0.19896
2.50005	0.00116	0.10502	0.9327	0.20182
2.75	0.00104	0.11063	0.8527	0.17932
2.99994	8.83193E-4	0.09775	0.78312	0.17811
3.24993	7.58355E-4	0.10465	0.72393	0.14891
3.49996	6.16703E-4	0.10693	0.67591	0.12118
3.74992	4.33585E-4	0.07622	0.62805	0.11632
3.99993	3.23559E-4	0.08242	0.58753	0.07998
4.24991	2.16892E-4	0.0534	0.55167	0.06177

COMPUTATIONAL DETAILS

All calculations were performed using the ORCA 4.2.1^{S25} software suite. We prepared a monomeric model and optimized the position of hydrogens using the BP86 level of theory^{S26, S27} with DKH-def2-SVP^{S28} basis set for all the atoms to extract the zero-field splitting parameters, g-value in complex **1**. The electronic, magnetic, and spin-Hamiltonian parameters (*g*, *D*, *E*) were calculated using the complete active space self-consistent (CASSCF)^{S29} method with an active space of CAS (7, 5), i.e., seven active electrons in the five active d-orbitals of Co. (II). We computed 10 quartets and 40 doublet states using this active space. All calculations were performed using a DKH-def2-TZVPP^{S28} basis set for Co and a DKH-def2-SVP basis set for all other atoms. On the converged CASSCF wavefunction, the second-order N-electron valence perturbation theory (NEVPT2)^{S30, S31} method was used to treat the dynamic correlations. To investigate the nature of ligand field and d-orbital splitting ab-initio based ligand field theory (AILFT) calculations were carried out as implemented in ORCA.

Table S11. CASSCF/NEVPT2 computed 10 spin-free quartet (red) and 40 spin-free doublet (blue) states along the spin-orbit states for Co centre in complex 1a. All the values are reported here in cm⁻¹

Complex 1a					
SPIN-FREE STATES		SPIN-ORBIT		STATES	
CASSCF	NEVPT2	CASSCF		NEVPT2	
0.0	0.0	0.00	26412.51	0.00	23113.49
265.6	398.7	247.00	26722.98	222.46	24779.11
508.6	608.2	469.26	28804.31	530.37	27099.15
5701.5	7411.4	883.08	29112.14	921.78	27430.42
6131.3	7998.2	1065.40	29371.21	1109.56	28046.89
7147.3	9258.9	1186.93	29443.22	1245.88	28130.29
13499.1	17340.7	6116.17	29711.50	7763.54	28568.47
22834.0	20739.7	6188.25	30202.58	7823.52	29315.15
23250.1	21241.0	6544.04	31705.10	8346.20	30669.73
24002.0	22132.2	6618.40	31872.76	8407.36	30939.89
14499.6	34113.1	9846.4	33136.8	7555.45	34328.01
15788.5	34187.4	11566.8	33303.7	7650.40	34456.52
19428.9	34289.2	17023.6	33369.1	13980.36	34635.87
19953.7	34623.0	17909.0	34374.6	13985.05	35073.53
20037.6	34698.7	17911.6	34583.0	14913.75	35180.66
20155.1	34793.9	18096.3	34792.5	16199.51	35327.77
20586.2	34841.0	18780.0	34963.1	19824.84	35737.02
20861.8	35120.4	19336.3	34992.9	20144.84	36085.79
24324.0	46532.3	21950.6	40351.0	20456.30	46868.64
25657.9	46826.1	22125.7	40827.0	20766.78	47306.15
25745.8	47124.6	22143.7	41295.2	21141.73	47647.93
25872.3	47563.0	24292.2	42511.2	21450.50	47996.66
28439.7	47717.3	26770.2	42715.9	23108.85	48132.46
28577.8	47962.4	26911.9	42991.4	23146.45	48512.95
28876.3	48581.5	27600.5	43364.6	23516.92	49064.69
28906.4	71731.6	27699.9	62767.8	23638.94	72169.83
29230.3	72024.1	28157.9	63336.2	24219.42	72478.51
29771.7	72376.7	28942.5	63643.4	24456.71	72799.32
31199.7	72633.6	30218.2	63897.5	24681.38	73198.93
31376.3	72863.1	30505.0	64098.3	26145.03	73408.68
					23057.28
					64602.20

Table S12. CASSCF (7,5)+NEVPT2 computed Spin – Hamiltonian parameter (g, D, |E/D|) along with listed state – by – state contribution to the D. All the values are reported here in cm⁻¹

Parameters	1	
	CASSCF	NEVPT2
	Contribution to D (cm ⁻¹)	
D	121.15	109.29
E/D	0.11	0.11
g _{xx}	1.850	1.900
g _{yy}	2.336	2.442
g _{zz}	2.961	2.783
KD1		
g _{xx}	3.102	2.782
g _{yy}	3.828	4.008
g _{zz}	6.134	6.065
KD2		
g _{xx}	0.522	0.737
g _{yy}	1.126	0.992
g _{zz}	4.826	5.221

EHA : Effective Hamiltonian approach

Table S13. AILFT derived ligand field parameters computed at NEVPT2 level of theory for model complexes **1**. The values of B, C, ξ and Δ_o parameters are provided in units of cm⁻¹.

Parameter	Free Co(II)	1	% reduction
ξ	530.3	520.4	1.87
B	1040.3	1005.7	3.33
C	4158.1	3909.0	5.99
C/B	3.997	3.887	2.75
Δ_o		7519.8	

Table S14. NEVPT2-AILFT computed d-orbital ordering for model complexes **1**.

Orbital	Energy (cm ⁻¹)
d _{yz}	0
d _{xz}	329.8
d _{xy}	593.2
d _{x²-y²}	7012.2
d _{z²}	8642.7

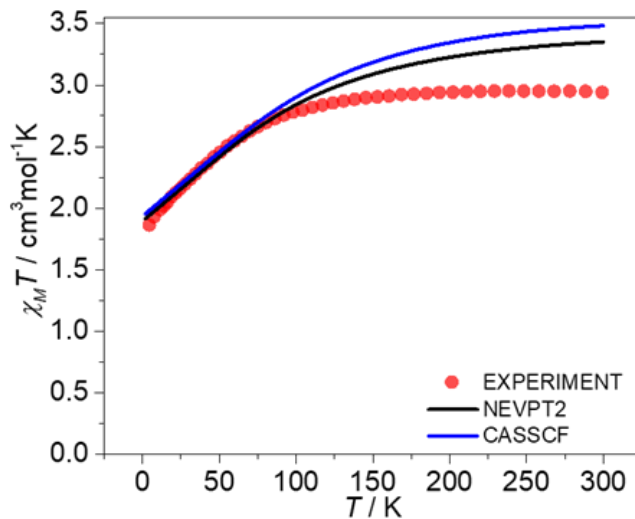


Figure S12. Experimental and ab initio computed molar magnetic susceptibility plots where red circles correspond to the experimental values and the blue and black lines correspond to CASSCF and NEVPT2 computed values respectively.

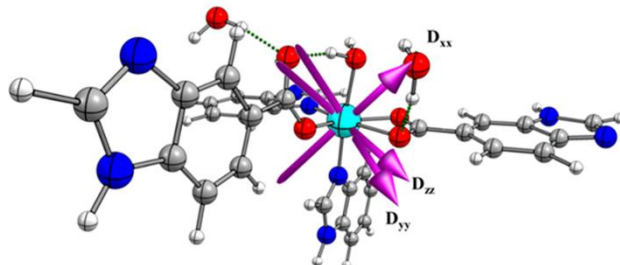
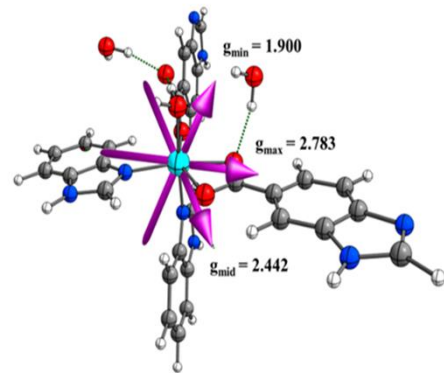


Figure S11. NEVPT2 computed orientation of computed effective g-tensor and D-tensor for complex **1**. Color code: Co(cyan), N (blue), C (grey), O(red), H(white).

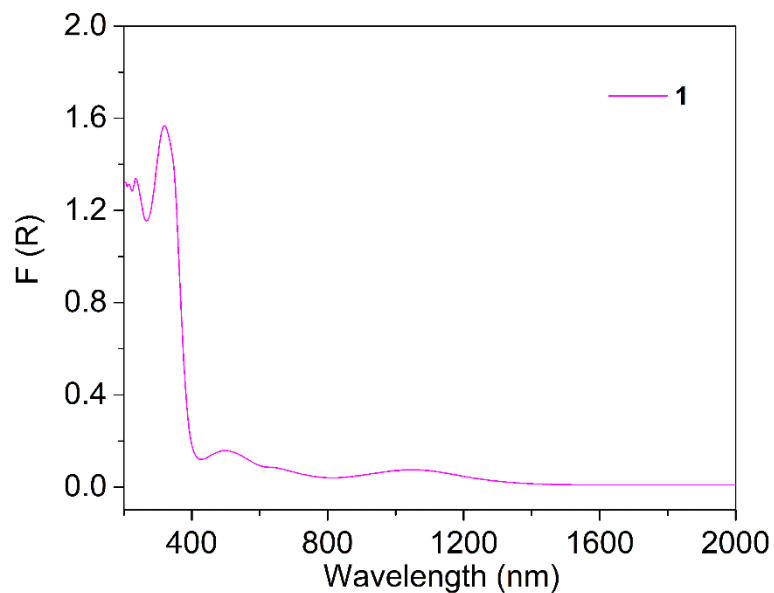


Figure S13. Solid-state UV-vis-NIR of **1**.

References

- S1) SAINT Software Users Guide, version 7.0; Bruker Analytical X-Ray Systems: Madison, WI, 1999.
- S2) G. M. Sheldrick, SADABS, version 2.03; Bruker Analytical X-Ray Systems, Madison, WI, 2000.
- S3) G. M. Sheldrick, SHELXTL, Version 6.14, Bruker AXS, Inc.; Madison, WI 2000-2003.
- S4) Dolomanov, O. V.; Bourhis, L. J.; Gildea, R. J.; Howard, J. A. K.; Puschmann, H. OLEX2: A Complete Structure Solution, Refinement and Analysis Program, *J. Appl. Crystallogr.*, 2009, 42, 339–341.
- S5) X. Liu, L. Sun, H. Zhou, P. Cen, X. Jin, G. Xie, S. Chen, and Q. Hu, Single-Ion-Magnet Behavior in a Two-Dimensional Coordination Polymer Constructed from Co^{II} Nodes and a Pyridylhydrazone Derivative, *Inorg. Chem.*, 2015, 54, 8884–8886.
- S6) J. Palion-Gazda, T. Klemens, B. Machura, J. Vallejo, F. Lloret and M. Julve, Single ion magnet behaviour in a two-dimensional network of dicyanamide-bridged cobalt(II) ions, *Dalton Trans.*, 2015, 44, 2989–2992.
- S7) Y.-L. Wang, L. Chen, C.-M. Liu, Y.-Q. Zhang, S.-G. Yin, and Q.-Y. Liu, Field-Induced Slow Magnetic Relaxation and Gas Adsorption Properties of a Bifunctional Cobalt(II) Compound, *Inorg. Chem.*, 2015, 54, 11362–11368.
- S8) A. K. Mondal, S. Khatua, K. Tomar and S. Konar, Field-Induced Single-Ion-Magnetic Behavior of Octahedral Co^{II} in a Two-Dimensional Coordination Polymer, *Eur. J. Inorg. Chem.*, 2016, 3545–3552.
- S9) L. Sun, S. Zhang, S. Chen, B. Yin, Y. Sun, Z. Wang, Z. Ouyang, J. Ren, W. Wang, Q. Wei, G. Xie and S. Gao, A two-dimensional cobalt(II) network with a remarkable positive axial anisotropy parameter exhibiting field-induced single-ion magnet behavior, *J. Mater. Chem. C*, 2016, 4, 7798–7808.
- S10) A. Świtlicka-Olszewska, J. Palion-Gazda, T. Klemens, B. Machura, J. Vallejo, J. Cano, F. Lloretb and M. Julve, Single-ion magnet behaviour in mononuclear and two-dimensional dicyanamide-containing cobalt(II) complexes, *Dalton Trans.*, 2016, 45, 10181–10193.
- S11) J. Vallejo, F. R. Fortea-Perez, E. Pardo, S. Benmansour, I. Castro, J. Krzystek, D. Armentanoc and J. Cano, Guest-dependent single-ion magnet behaviour in a cobalt(II) metal–organic framework, *Chem. Sci.*, 2016, 7, 2286–2293.
- S12) Y.-L. Wang, L. Chen, C.-M. Liu, Z.-Y. Du, L.-L. Chen and Q.-Y. Liu, 3D chiral and 2D achiral cobalt(II) compounds constructed from a 4-(benzimidazole-1-yl)benzoic ligand exhibiting field-induced single-ion-magnetttype slow magnetic relaxation, *Dalton Trans.*, 2016, 45, 7768–7775.
- S13) R. Ma, Z. Chen, F. Cao, S. Wang, X. Huang, Y. Li, J. Lu, D. Lia and J. Dou, Two 2-D multifunctional cobalt(II) compounds: field-induced single-ion magnetism and catalytic oxidation of benzylic C–H bonds, *Dalton Trans.*, 2017, 46, 2137–2145.
- S14) A. Rodríguez-Díéguez, S. Pérez-Yáñez, L. Ruiz-Rubio, J. M. Seco and J. Cepeda, From isolated to 2D coordination polymers based on 6-aminonicotinate and 3d-metal ions: towards field-induced single-ion-magnets, *CrystEngComm*, 2017, 19, 2229–2242.
- S15) D. Shao, L. Shi, H.-Y. Wei and X.-Y. Wang, Field-Induced Single-Ion Magnet Behaviour in Two New Cobalt(II) Coordination Polymers with 2,4,6-Tris(4-pyridyl)-1,3,5-triazine, *Inorganics*, 2017, 5, 90.
- S16) L. Shi, D. Shao, H.-Y. Wei and X.-Y. Wang, Two Interpenetrated Cobalt(II) Metal–Organic Frameworks with Guest-Dependent Structures and Field-Induced Single-Ion Magnet Behaviors, *Cryst. Growth Des.* 2018, 18, 5270–5278.
- S17) D. Ma, G. Peng, Y.-Y. Zhang and B. Li, Field-induced slow magnetic relaxation in

- twodimensional and three-dimensional Co(II) coordination polymers, *Dalton Trans.*, 2019, 48, 15529–15536.
- S18) M. A. Palacios, I. F. Díaz-Ortega, H. Nojiri, E. A. Suturina, M. Ozerov, J. Krzystek, E. Colacio, Tuning magnetic anisotropy by the π -bonding features of the axial ligands and the electronic effects of gold(I) atoms in 2D $\{\text{Co}(\text{L})_2[\text{Au}(\text{CN})_2]_2\}_n$ metal–organic frameworks with field-induced single-ion magnet behaviour, *Inorg. Chem. Front.*, **2020**, 7, 4611–4630.
- S19) Y.-R. Qiu, B. Li, Y. Zhou, J. Su and J.-Y. Ge, Pillar–template strategy switching the redox activity and magnetic properties of trisphenylamine-based coordination polymers, *CrystEngComm*, **2020**, 22, 3155–3163.
- S20) A. K. Kharwar, A. Mondal and S. Konar, Alignment of axial anisotropy of a mononuclear hexa-coordinated Co(II) complex in a lattice shows improved single molecule magnetic behavior over a 2D coordination polymer having a similar ligand field, *Dalton Trans.*, **2021**, 50, 2832–2840.
- S21) D. Shao, Y. Zhou, Q. Pi, F.-X. Shen, S.-R. Yang, S.-L. Zhang and X.-Y. Wang, Two-dimensional frameworks formed by pentagonal bipyramidal cobalt(II) ions and hexacyanometallates: antiferromagnetic ordering, metamagnetism and slow magnetic relaxation, *Dalton Trans.*, **2017**, 46, 9088–9096.
- S22) D. Shao, S. Moorthy, X. Yang, J. Yang, L. Shi, S. K. Singh and Z. Tian, Tuning the structure and magnetic properties via distinct pyridine derivatives in cobalt(II) coordination polymers, *Dalton Trans.*, **2022**, 51, 695–704.
- S23) L. Shi, F.-X. Shen, D. Shao, Y.-Q. Zhang and X.-Y. Wang, Syntheses, structures, and magnetic properties of three two-dimensional cobalt(II) single-ion magnets with a $\text{Co}^{II}\text{N}_4\text{X}_2$ octahedral geometry, *CrystEngComm*, **2019**, 21, 3176–318540.
- S24) X.-Q. Wei, D. Shao, C.-L. Xue, X.-Y. Qu, J. Chai, J.-Q. Li, Y.-E. Du, Y.-Q. Chen, Field-induced slow magnetic relaxation in two interpenetrated cobalt(II) metal–organic framework isomers, *CrystEngComm*, **2020**, 22, 5275–5279.
- S25) Neese, F. Software Update: The ORCA Program System, Version 4.0. *Wiley Interdiscip. Rev. Comput. Mol. Sci.* **2018**, 8 (1), 1–6.
- S26) Perdew, J. P. Density-Functional Approximation for the Correlation Energy of the Inhomogeneous Electron Gas. *Phys. Rev. B* **1986**, 33, 8822–8824.
- S27) Becke, A. D. Density-Functional Exchange-Energy Approximation with Correct Asymptotic Behavior. *Phys. Rev. A* **1988**, 38, 3098–3100.
- S28) Weigend, F.; Ahlrichs, R. Balanced Basis Sets of Split Valence, Triple Zeta Valence and Quadruple Zeta Valence Quality for H to Rn: Design and Assessment of Accuracy. *Phys. Chem. Chem. Phys.* **2005**, 7 (18), 3297–3305.
- S29) Malmqvist, P. Å.; Roos, B. o. THE CASSCF STATE INTERACTION METHOD. *Chem. Phys. Lett.* **1989**, 155, 189–194.
- S30) Angeli, C.; Cimiraglia, R. N -Electron Valence State Perturbation Theory : A Fast Implementation of the Strongly Contracted Variant. *Chem. Phys. Lett.* **2001**, 350, 297–305.
- S31) Angeli, C.; Cimiraglia, R.; Malrieu, J. N-Electron Valence State Perturbation Theory : A Spinless Formulation and an Efficient Implementation of the Strongly Contracted and of the Partially Contracted Variants. *J. Chem. Phys.* **2002**, 9138–9153.